Hindawi
Journal of Sensors
Volume 2021, Article ID 6950281, 11 pages
https://doi.org/10.1155/2021/6950281

Research Article

Composition Regulation and Microstructure Characterization of $Fe_{100-x}Ga_x$ Films in the Manufacturing Industry

Zhi Shen,[1,2] **Jian-Wu Yan**,[1,2] **Kang Jin**,[3] **Kai Fu**,[2] **and Ying-Li Zhou**[4]

[1]*School of Mechanical Engineering, Nanchang Institute of Technology, Nanchang 330099, China*
[2]*Jiangxi Province Key Laboratory of Precision Drive and Control, Nanchang 330099, China*
[3]*Beijing Research Institute of Mechanical & Electrical Technology Ltd., Beijing 100083, China*
[4]*Beijing National Innovation Institute of Lightweight Ltd., Beijing 100083, China*

Correspondence should be addressed to Zhi Shen; nickshen009@163.com

Received 5 August 2021; Revised 19 August 2021; Accepted 27 September 2021; Published 19 October 2021

Academic Editor: Kelvin Wong

$Fe_{100-x}Ga_x$ giant magnetostrictive films (GMF) are attracting ever increasing attention for their potential application to manufacturing integrated magnetostrictive displacement sensors. However, it is difficult to fabricate $Fe_{100-x}Ga_x$ thin films with different compositions at will. The influence of compositions on alloy phases, grain sizes, film surface roughness, and magnetic domains of the films and magnetization of magnetron sputtered $Fe_{100-x}Ga_x$ films was investigated. Changing the ratio of the pure iron slice areas to alloy target areas, the desired film composition was achieved by the improved Mosaic method. The morphologies, magnetic domain structure, microstructure, and compositions of $Fe_{100-x}Ga_x$ films revealed by SEM, EDS, XRD, MFM, VSM, and TEM. The results show that there are <1 1 0> texture in magnetron sputtered $Fe_{100-x}Ga_x$ films. The sharp peak attributed to the A_2 microstructure suggests that the film is crystalline. The magnetic domain structure of $Fe_{100-x}Ga_x$ films presents a network form, and the domain width decreases with the decrease of gallium content. It is also found that the magnetic domains of the films are not uniform. The TEM result shows that there are some strip patterns in the films, and the diffraction ring is discontinuous because of the structure extinction. For a suitable candidate of microdevice applications in MEMS, the optimum composition film should be $Fe_{83.25}Ga_{16.75}$ film.

1. Introduction

$Fe_{100-x}Ga_x$ giant magnetostrictive films (GMF) are attracting ever increasing attention for their potential application to manufacturing integrated magnetostrictive displacement sensors [1–3]. So, $Fe_{100-x}Ga_x$ films are the suitable candidate of other magnetostrictive materials, e.g., Terfenol-D and Fe-Ga alloy, because of its superior synthetic properties [4]. $Fe_{100-x}Ga_x$ films for microsensor and microactuator development are possible [5].

Magnetron sputtering is a commonly technology used to prepare giant magnetostrictive films [6, 7]. Magnetron sputtering has the advantages of fast deposition rate, strong adhesion between coating and substrate, compact, and uniform coating.

Film grain size will be small and as well as surface roughness will be decrease when the substrates were maintained at lower temperature. This is beneficial to improve the performance of thin films. Basumatary et al. report the microstructure and magnetic properties of $Fe_{100-x}Ga_x$ films deposited at different deposited temperatures [5]. The grain size and surface roughness increase with the increasing of substrate temperature. The films deposited at higher substrate temperatures were found to saturate at lower magnetic field as compared to the room temperature deposited film. X-ray diffraction and TEM results revealed the presence of disordered A_2 phase in the films.

Preparing thin films is crucial to developing microdevices. The thin-film physical, mechanical, and chemical properties depend on how the film structure is organized, which is closely related to film composition [8, 9].

Single-metal-target and single-alloy-target sputtering are often used to fabricate various alloy thin films [10, 11].

However, traditional elemental-target co-sputtering cannot be used to prepare $Fe_{100-x}Ga_x$ films because gallium shows a low melting point. As a sputtering target, it is difficult to exist stably above room temperature. In addition, it is expensive and difficult to develop a series of $Fe_{100-x}Ga_x$ alloy targets because smelting $Fe_{100-x}Ga_x$ is a little difficult. There are some technology problems when $Fe_{100-x}Ga_x$ alloy targets prepared by melting, which means it is difficult to tune compositions of $Fe_{100-x}Ga_x$ films precisely at will.

So-called mosaic targets, *i.e.*, targets whose matrices consist of one metal and whose inserts consist of others, have recently been used to develop methods of magnetron-sputtering multicomponent thin films [12].

Such effective methods rely on several components being limited to fabricate numerous multicomponent alloy thin films. However, the traditional mosaic target must be drilled in order to embed the second material on the surface of the matrix target, which will produce gap on the target, affect the electromagnetic field uniformity, and affect the sputtering process. Against this background, Yan et al. report a composite or improved mosaic targets to tune $Fe_{100-x}Ga_x$ film compositions [13].

The way to do that is pure-iron patch is magnetically attracted to the surface of the $Fe_{100-x}Ga_x$ alloy target that can be a minitarget, and the $Fe_{100-x}Ga_x$ alloy target was another sputter target whose sputter area is reduced. Iron slices cover $Fe_{100-x}Ga_x$ alloy target surface, shielding it from Ar^+ bombardment, so the iron slices are bombarded instead of its increased surface area, assuming all other sputtering conditions are the same. Hence, the sputtered $Fe_{100-x}Ga_x$ films will be composite of a small amount of iron atoms come from the iron target and $Fe_{100-x}Ga_x$ alloy come from the $Fe_{100-x}Ga_x$ alloy target.

This, in essence, is equivalent to increasing the iron content in the target material, which subsequently increases the iron content in the sputtered film. Further, increasing the sputter area per unit of time increases the probability that the iron slices will be bombarded with argon ions so that more iron atoms are sputtered onto the target. The sputtering principle how to influence on film compositions must be further discussed.

In the process of magnetron sputtering, electrons collide with argon atoms and ionize a large number of argon ions and electrons, and the electrons fly to the substrate. A large number of target atoms are sputtered out by argon ions under the action of electric field, and the neutral target atoms (or molecules) are deposited on the substrate.

However, the nonuniform distribution of the magnetic field on the target surface leads to the nonuniform etching on the target surface, and the argon ion bombards the target surface selectively, and the intensity of bombardment is high in some places and weak in others; therefore, a deep circular groove is formed on the round target surface, which is located at the quarter of the diameter of the target surface. Therefore, the location of the pure patch on the target should be in the etching region in order to effectively control the composition of the sputtering film.

Films with high effective saturation magnetostriction constant and low stress fabricated by magnetron sputtering when argon pressure is suitable [14]. Liu et al. reported that the modified-DO_3 phase and the (100) texture play a positive role in magnetostrictive properties of $Fe_{77}Ga_{23}$ ribbons [15]. Some investigations reported that preparation methods affect magnetic properties of Fe-Ga films [16].

It is of great theoretical value to study the microstructure of magnetic domains, which is the basic physical parameter of magnetic materials. Magnetic domains or defects in ferromagnetic materials can be identified by magnetic imaging.

The domain structures of TbFe and Terfenol-D magnetostrictive thin films were investigated by Shih et al. [17] and Song et al. [18]. Sun et.al reported the magnetic properties and domain structures of FeSiB prepared by RF-sputtering method [19]. However, up to now, the domain structure of $Fe_{100-x}Ga_x$ films has been seldom reported.

It is well known that the magnetic domain structure affects magnetic properties of $Fe_{100-x}Ga_x$ films. MFM is an effective instrument to observe the magnetic structure of magnetic films. The MFM can give the magnetic domain image and surface roughness, come from the interaction between magnetic charges of the sample surface and magnetic probe.

In order to enhance these material analyses and optimize the concentration as well as better understand the influence of compositions on microstructure, deep learning [20] may be applied to assist in our study. Some advanced technologies [21, 22] in other fields can also be used for reference to develop new sensing technologies. It is centered on the simple mosaic targets to prepare $Fe_{100-x}Ga_x$ films in this paper. The purpose is composition regulation and microstructure characterization of $Fe_{100-x}Ga_x$ films.

2. Materials and Methods

A direct current (DC) magnetron sputtering equipment (JZCK-600F) was adopted to deposit films. The sputtering chamber base pressure was 2×10^{-4} Pa, and 0.6 Pa argon (99.99% pure) was used during sputtering. 90 W sputtering power and 70 minutes sputtering time were chosen. The vertical distance between the target and the substrate was 100 mm. The substrates were maintained at room temperature.

In the experiment, some polished glasses were chosen as the substrates to deposit films. Its surfaces were cleaned by ultrasonic before sputtering. The thickness of films can be calculated by the weighing method [23]. The average value is taken as the thickness of films to reduce errors in the experiment.

$Fe_{84}Ga_{16}$ alloy target was used to prepare $Fe_{100-x}Ga_x$ films. The diameter of target is 60 mm, and its thickness is 3 mm. Some pure iron slices were absorbed to the etching area of round $Fe_{84}Ga_{16}$ alloy target by magnetron force, which is located at the quarter of the diameter of the target surface. The purity of iron slices used in the experiment was 99.99% and distributed uniformly on the target. The desired film composition was achieved by changing the ratio of the pure iron slice areas to alloy target areas (i.e., the area ratio, R).

The surfaces of $Fe_{100-x}Ga_x$ films were coated with gold. Scanning electron microscopy (SEM, Quanta 200) was used to characterize the surface morphologies of the gold-coated $Fe_{100-x}Ga_x$ films. The average composition and distributions of elements on the surfaces of $Fe_{100-x}Ga_x$ films were determined by an energy dispersive spectroscopy (EDS, Oxford energy-scattering spectrometer).

Bruker AXS D8 ADVANCE X-ray diffractometer (XRD) was used to analyze the film phase. X-ray tube target is Cu target, voltage is 40.0 (kV), and current is 30.0 (mA). Divergence slit is 1.00000 (deg), scatter slit is 1.00000 (deg), and receiving slit is 0.30000 (mm). Scan speed is 7.0000 (deg/-min), sampling pitch is 0.0200 (deg), and preset time is 0.17 (sec).

The magnetic domain structure of $Fe_{100-x}Ga_x$ films was observed by a magnetic force microscopy (MFM, Micro-Nano D5A); the scan rage is 5 micron meter~10 micron meter.

The specimens no. (a) and no. (f) were deposited on polished glass; then, the films were removed from the glass and observed by a Jeol-2010F transmission electron microscope (TEM).

A YP07 vibrating sample magnetometer (VSM) was adopted to test magnetic hysteresis loop of $Fe_{100-x}Ga_x$ films.

A theoretical equation can be used to calculate film compositions. The theoretical formula of film composition can be deduced as follows [23].

According to the sputtering principle, the total material which sputtering on the substrate surface can be expressed as follows:

$$Q \approx \frac{k_1 Q_0}{qH}, \tag{1}$$

where k_1 is the constant value, q is the sputtering pressure, and H represents the target-substrate distance. Q_0 is the magnitude of target sputtering which can be approximated as:

$$Q_0 \approx \left(\frac{I_+}{e}\right) \mathrm{St}\left(\frac{M}{N}\right), \tag{2}$$

where I_+ is the current of target ion, e is the charge of an electron, S is the sputtering rate, t is the sputtering time, M is the atomic weight of sputtered materials, and N is the Avogadro constant. Generally speaking, the discharge current I_S may be close to I_+ when sputtering, and there is a formula as follows:

$$S \propto V_s, \tag{3}$$

where V_S is the discharge voltage. However, the relationship between Q_0 and A (the area of target material) can be expressed within the scope of sputtering as follows:

$$Q_0 \propto A. \tag{4}$$

Therefore, Q_0 can be approximated as:

$$Q_0 \approx k_2 V_s I_s t A, \tag{5}$$

where k_2 is the constant of target material. According to formulas (1) and (5), the total of sputtered material can be represented as:

$$Q \approx \frac{k_1 k_2 V_s I_s t A}{qH} = \frac{k V_s I_s t A}{qH}. \tag{6}$$

From this expression, it can be seen that the total amount of sputtered materials from metal substrate is in direct proportion to electric energy ($V_S I_S t$) consumed on the device and the areas of target material (A). And it is inversely proportional to the sputtering pressure and the vertical distance between the target and the substrate.

Therefore, for mosaic target sputtering, the total amount of sputtered materials from the substrate can be approximated as:

$$Q \approx Q_{\mathrm{Fe}} + Q_{\mathrm{Fe\text{-}Ga}}. \tag{7}$$

Combined formulas (6) and (7), it can be given as follows:

$$Q \approx \frac{(k_{\mathrm{Fe}} V_{\mathrm{Fe}} I_{\mathrm{Fe}} A_{\mathrm{Fe}} + k_{\mathrm{Fe\text{-}Ga}} V_{\mathrm{Fe\text{-}Ga}} I_{\mathrm{Fe\text{-}Ga}} A_{\mathrm{Fe\text{-}Ga}}) t}{qH}. \tag{8}$$

Considering that sputtering power can be calculated by formula (9), it can be expressed by formula (10).

$$P = V_S I_S, \tag{9}$$

$$Q \approx \frac{(k_{\mathrm{Fe}} P_{\mathrm{Fe}} A_{\mathrm{Fe}} + k_{\mathrm{Fe\text{-}Ga}} P_{\mathrm{Fe\text{-}Ga}} A_{\mathrm{Fe\text{-}Ga}}) t}{qH} = Q_{\mathrm{Fe}} + Q_{\mathrm{Fe\text{-}Ga}}, \tag{10}$$

where k_{Fe} is a coefficient related to iron element target sputtering, $k_{\mathrm{Fe-Ga}}$ is a coefficient in relation to $Fe_{100-x}Ga_x$ target sputtering, P_{Fe} and $P_{\mathrm{Fe-Ga}}$ severally denote sputtering powers of iron element target and $Fe_{100-x}Ga_x$ targets, A_{Fe} and $A_{\mathrm{Fe-Ga}}$, respectively, signify the areas of iron element target and uncovered $Fe_{100-x}Ga_x$ targets. In the mosaic target sputtering, iron slices are attached on the $Fe_{100-x}Ga_x$ targets, and they have the same target seats, so it can be considered that P_{Fe} is equal to $P_{\mathrm{Fe-Ga}}$, and they all equal sputtering power (P).

Thus, Q can be approximated as follows:

$$Q \approx \frac{(k_{\mathrm{Fe}} A_{\mathrm{Fe}} + k_{\mathrm{Fe\text{-}Ga}} A_{\mathrm{Fe\text{-}Ga}}) P t}{qH} = Q_{\mathrm{Fe}} + Q_{\mathrm{Fe\text{-}Ga}}. \tag{11}$$

In the experiment, iron content in the $Fe_{100-x}Ga_x$ films derives from two aspects. On the one hand, it is from pure iron slices. On the other hand, it comes from uncovered $Fe_{100-x}Ga_x$ targets. However, gallium content only stems from the $Fe_{100-x}Ga_x$ target. Thus, the relative contents of

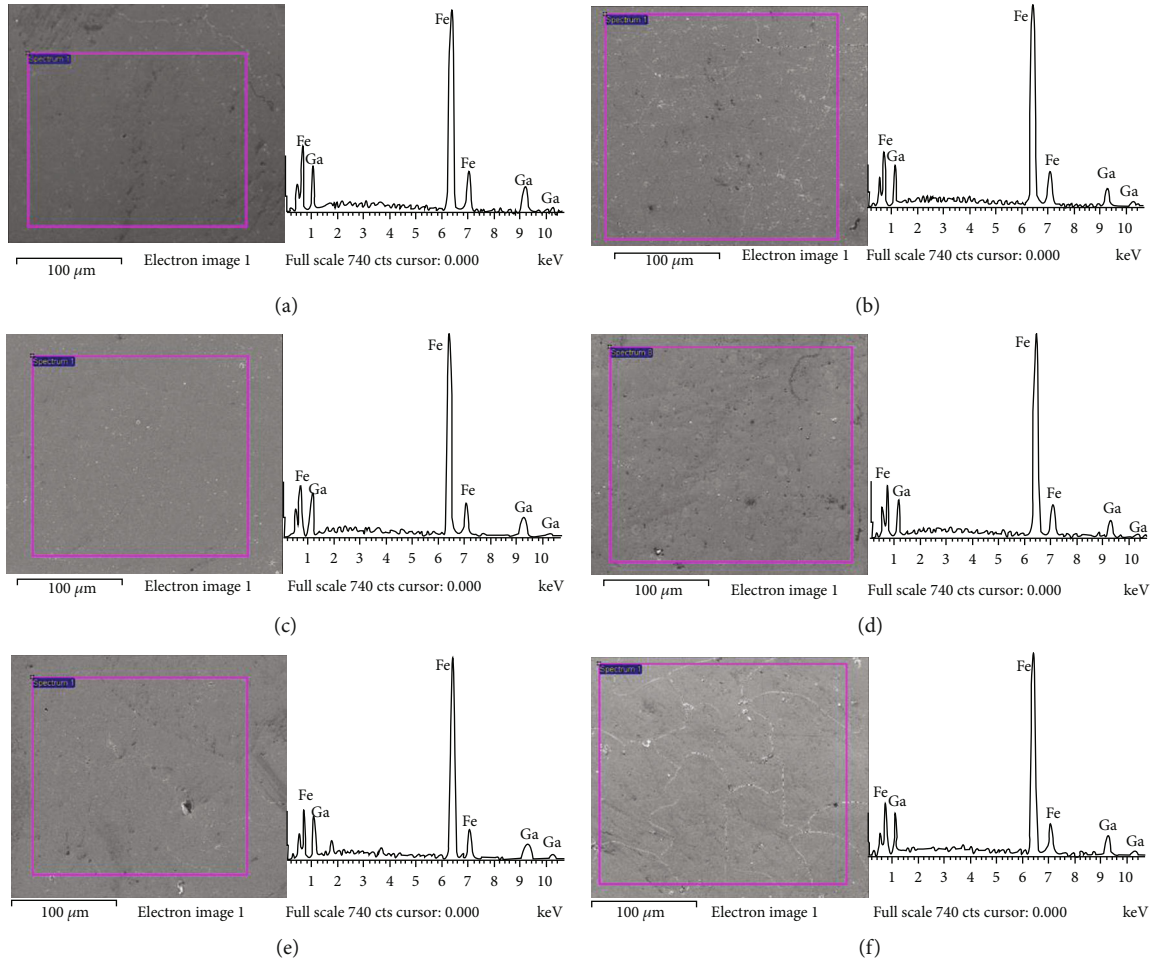

FIGURE 1: EDS results of as-deposited $Fe_{100-x}Ga_x$ films: (a_1, a_2) $R = 0$, (b_1, b_2) $R = 0.014$, (c_1, c_2) $R = 0.028$, (d_1, d_2) $R = 0.042$, (e_1, e_2) $R = 0.056$, and (f_1, f_2) $R = 0.070$.

iron and gallium of $Fe_{100-x}Ga_x$ films can be expressed as formula (12) and formula (13).

$$M_{Fe}\% = \frac{Q_{Fe} + Q_{Fe\text{-}Ga} \cdot m_{Fe}\%}{Q}, \tag{12}$$

$$M_{Ga}\% = \frac{Q_{Fe\text{-}Ga} \cdot m_{Ga}\%}{Q}, \tag{13}$$

where $m_{Fe}\%$ and $m_{Ga}\%$, respectively, mean iron and gallium content in the sputtered films from $Fe_{100-x}Ga_x$ targets uncovered with iron, and $M_{Fe}\%$ and $M_{Ga}\%$ separately represent the actual content of iron and gallium in the sputtered films.

Formulas (14) and (15) are given by means of substituting expression (11) into formulas (12) and (13).

$$M_{Fe}\% = \frac{k_{fe}A_{fe} + k_{fe\text{-}Ga}A_{fe\text{-}Ga} \cdot m_{Fe}\%}{k_{fe}A_{fe} + k_{fe\text{-}Ga}A_{fe\text{-}Ga}}, \tag{14}$$

$$M_{Ga}\% = \frac{k_{fe\text{-}Ga}A_{fe\text{-}Ga} \cdot m_{Ga}\%}{k_{fe}A_{fe} + k_{fe\text{-}Ga}A_{fe\text{-}Ga}}, \tag{15}$$

where $m_{Fe}\%$ and $m_{Ga}\%$ represent the content of iron and gallium in the pure $Fe_{100-x}Ga_x$ targets sputtering, separately.

On the basis of formulas (14) to (17), formulas (18) and (19) can be easily inferred.

$$A_{Fe\text{-}Ga} = A_{Target} - A_{Fe}, \tag{16}$$

$$R = \frac{A_{Fe}}{A_{Target}}, \tag{17}$$

$$M_{Fe}\% = \frac{k_{Fe}R + k_{Fe\text{-}Ga}(1-R)m_{Fe}\%}{k_{Fe}R + k_{Fe\text{-}Ga}(1-R)}, \tag{18}$$

$$M_{Ga}\% = \frac{k_{Fe\text{-}Ga}(1-R)m_{Ga}\%}{k_{Fe}R + k_{Fe\text{-}Ga}(1-R)}. \tag{19}$$

To calculate the correlation coefficients k_{Fe} and $k_{Fe\text{–}Ga}$, experimental data measured by EDS can be applied to formulas (18) and (19). And then, the calculation values of iron content and gallium content can be calculated when different R values were chosen. Conversely, we can use this formula to calculate the area ratio R when we want to sputter a thin film of a certain composition and thus determine how many pieces of iron are needed.

Table 1: EDS results of as-deposited $Fe_{100-x}Ga_x$ films.

Specimen no.	a	b	c	d	e	f
R, area ratio of iron slices to alloy targets	0	0.014	0.028	0.042	0.056	0.070
Fe content in films, at.100%	83.25	83.61	84.35	84.58	84.95	85.48
Ga content in films, at.100%	16.75	16.39	15.65	15.42	15.05	14.52

This model can be used to implement the preparation of thin films with different compositions, accurately predict, and precisely tune the composition of thin films.

3. Results and Discussion

3.1. EDS Analysis of $Fe_{100-x}Ga_x$ Films. The thickness of $Fe_{100-x}Ga_x$ films was about 1 μm. Morphologies and EDS spectra of as-deposited $Fe_{100-x}Ga_x$ films are shown in Figure 1. The area ratio of iron slices and alloy targets was defined as *R*. The relationship between the ratio *R* and the iron content and gallium content in $Fe_{100-x}Ga_x$ films is demonstrated in Table 1 and Figure 2. It can be observed that iron content in $Fe_{100-x}Ga_x$ films increases with increasing the value *R* and approximately linearly related.

However, the experimental results show that the compositions of specimen no. (a) are not the same to the compositions of the target. When the film of specimen no. (a) was prepared by magnetron sputtering, pure iron patches were not attached to the Fe84Ga16 alloy target. Why is the content of iron in the film lower than that in the target?

The composition of the films depends on the sputtering rate of the atoms, and the sputtering rate depends on the threshold energy and the sputtering power of the target. The content of the elements with high sputtering rate is higher in the sputtering film. The sputtering rate of gallium is higher than that of iron, which results in this phenomenon.

The compositions of $Fe_{100-x}Ga_x$ films depend on the alloy target compositions when a single alloy sputtering targets is used for magnetron sputtering. Nevertheless, it relies on sputtering cases of every target when composite or mosaic targets were used for sputtering. It hinges on the area ratio between the slices and the target employing the slice-style mosaic target for sputtering.

This can be explained by the surface free energy theory. The iron atom has a radius of 1.24 Å, the outer electron 3d64s2.Ga has a radius of 1.4 Å, and the outer electron is 4s2p1. The iron atom's outermost electron, 4s2, is saturated and has a smaller radius than the gallium atom. As a result, the outermost electrons of gallium are more easily lost than those of Fe and require lower energy to ionize, so the excitation voltage is lower than that of Fe.

At the same time, since the surface binding energy of iron is higher than that of gallium and the binding force between the atoms is greater, the kinetic energy of iron atoms or clusters from the surface of iron target to be sprayed by ionized gas ions is higher than that of gallium target; that is, a higher discharge voltage is required. Therefore, the discharge voltage of magnetron sputtering and the surface binding energy (Es) of target increase. The greater the sputtering yield of an element, the higher the content of the element in the film.

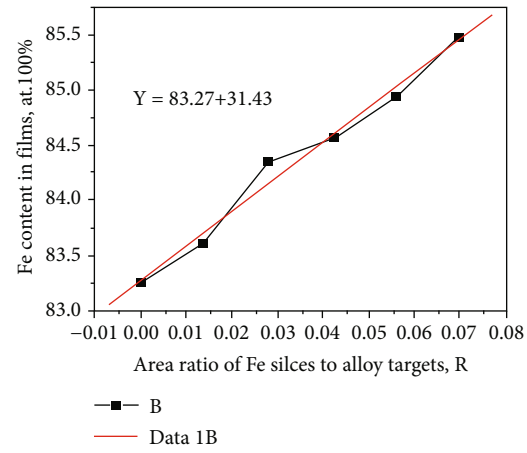

Figure 2: The relationship between the area ratio *R* and content of iron element in $Fe_{100-x}Ga_x$ films.

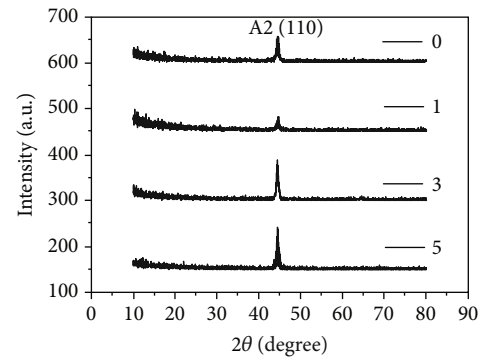

Figure 3: X-ray diffraction patterns of as-deposited $Fe_{100-x}Ga_x$ films.

3.2. XRD Analysis of Fe-Ga Alloy Films. Figure 3 shows XRD patterns of $Fe_{100-x}Ga_x$ films. The results show that there are <1 1 0> texture in magnetron sputtered $Fe_{100-x}Ga_x$ films. The sharp peak attributed to the A_2 microstructure suggests that the film is crystalline. However, the XRD peak of A_2 in $Fe_{100-x}Ga_x$ films is weak.

The experimental conditions are the incident light intensity, the sample area, the counting time per step, the opening size of the detector end, etc. When the experimental conditions are the same, the volume percent content of a phase in the sample is related to the intensity of its diffraction peak. Under the conditions determined by the Absorption Lorentz factor and the temperature factor, the content of a phase in the sample is directly proportional to the intensity of its

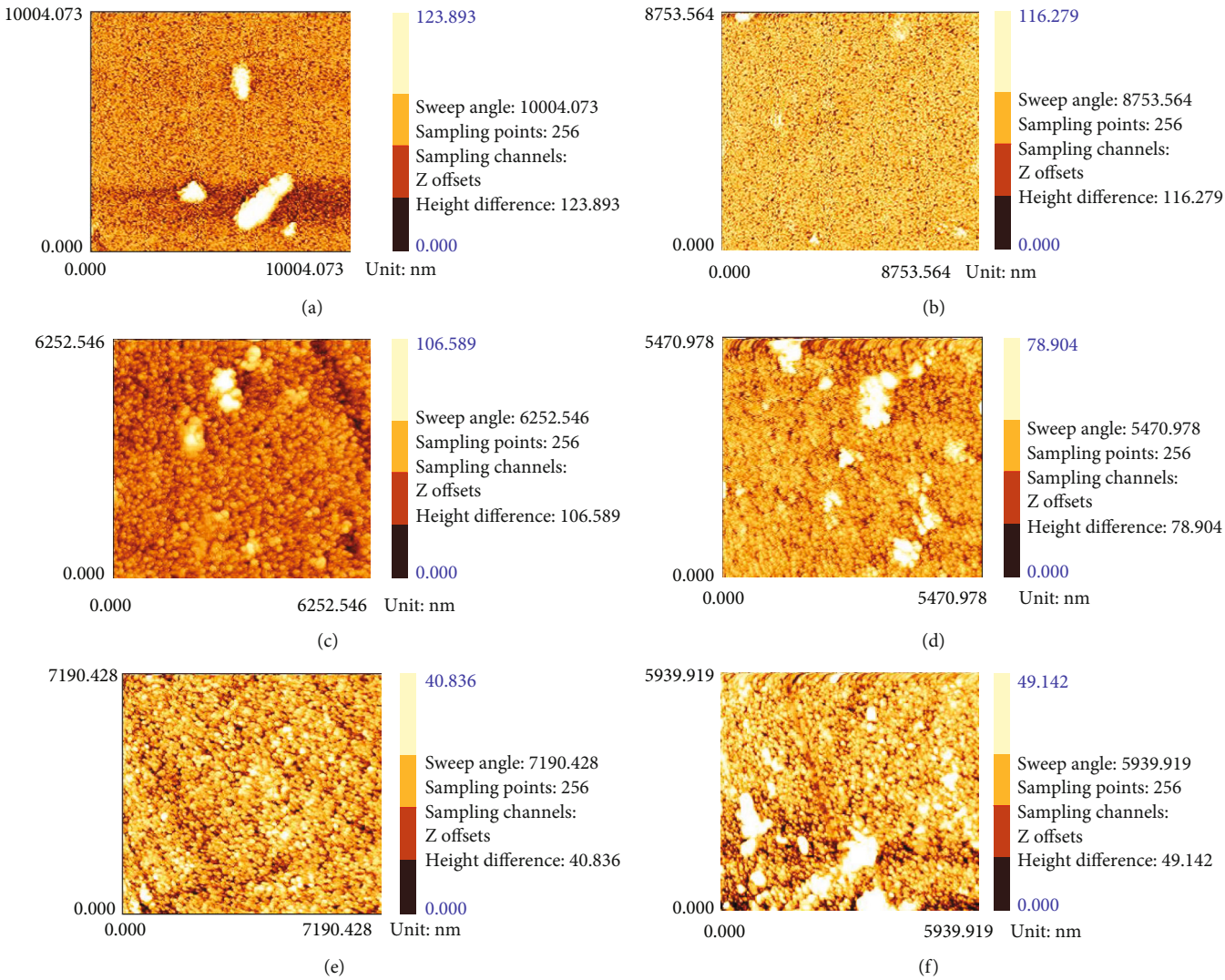

Figure 4: Domain structure of $Fe_{100-x}Ga_x$ films.

diffraction peak. In addition, the degree of crystal development and the preferred orientation of crystal plane also affect the intensity of characteristic diffraction peak.

Under the experimental conditions, there is only one A_2 (110) strong diffraction peak in Figure 3, which indicates that the sample has preferred orientation; all films are in polycrystalline form with <1 1 0>crystallographic texture perpendicular to the film plane.

The diffraction peak intensity was related to the film microstructure. In order to obtain fine grain and microstructure, the thin films were prepared by low sputtering energy, multiple sputtering, and 5 minutes interval. Therefore, the substrate temperature will not be too high. Then, the crystallization process can not be completed because of the weak diffusion ability of atoms.

Under this experimental condition, mixed structures, including crystalline and amorphous structures, will be formed. Most of the stress in the alloy film can be removed if heat treatment is carried out in the subsequent process. Driven by temperature gradient and residual stress, the atoms in the films may migrate and segregate. When the annealing temperature reaches a certain critical value, the atoms in the film will be formed with large area arranged in order.

In general, a variety of phase structures, such as A_2 structure and DO_3 structure, may be formed during the preparation of $Fe_{100-x}Ga_x$ films. However, there is no obvious evidence of DO_3 phase formation from the abovementioned testing process. It has been reported in the literature that the formation of DO_3 phase depends mainly on the thickness of the film [14, 24]. The reason why the DO_3 phase was not found in the study may be that the peak value was too weak to be detected. Kumagai reported that when the content of gallium in Fe-Ga alloy varies from 15% to 30%, the A_2, DO_3, $L1_2$, B_2, and DO_{19} phase structures appear under different preparation conditions [25]. At room temperature, when gallium content in Fe-Ga alloy exceeds its solubility, gallium atoms will exist in the form of clusters, while the main body of Fe-Ga material still retains the Bcc phase of alpha iron; the BCC phase gradually changed to DO_3 phase,

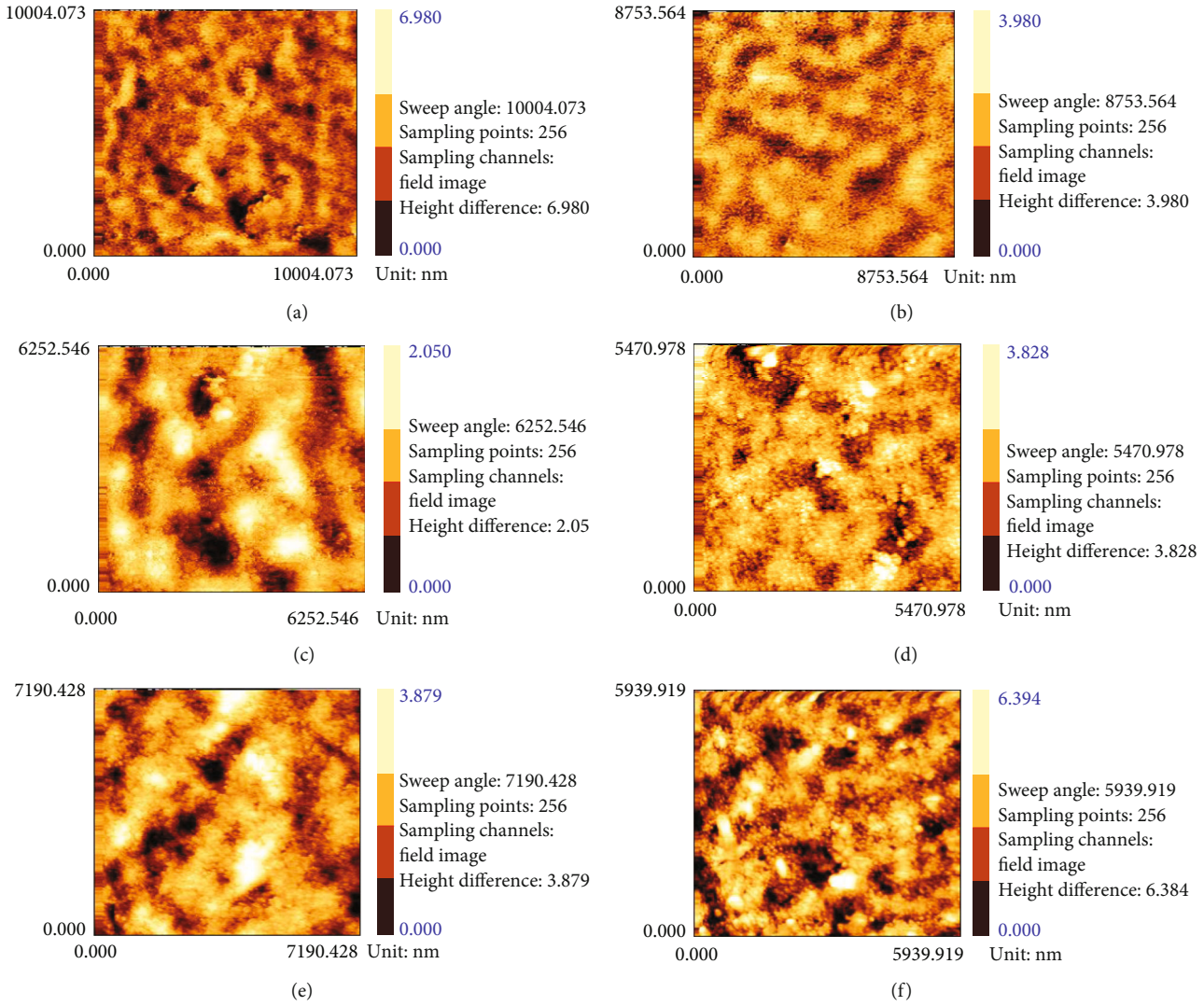

Figure 5: AFM image of $Fe_{100-x}Ga_x$ films.

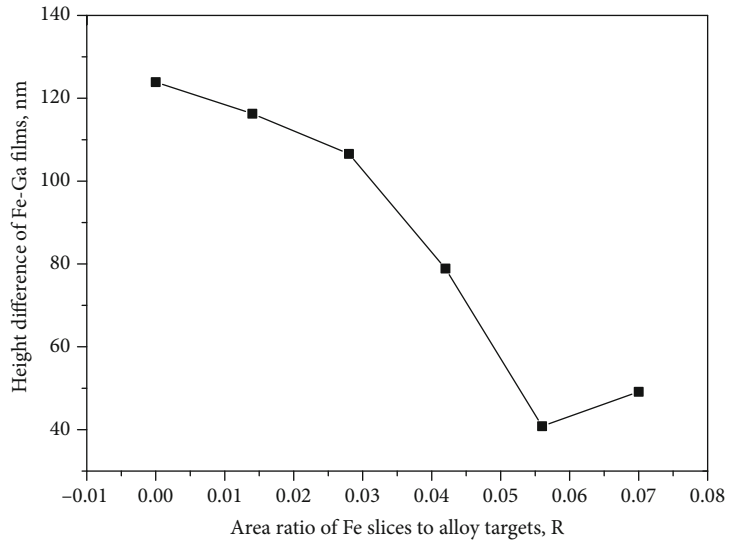

Figure 6: Height difference of the $Fe_{100-x}Ga_x$ films.

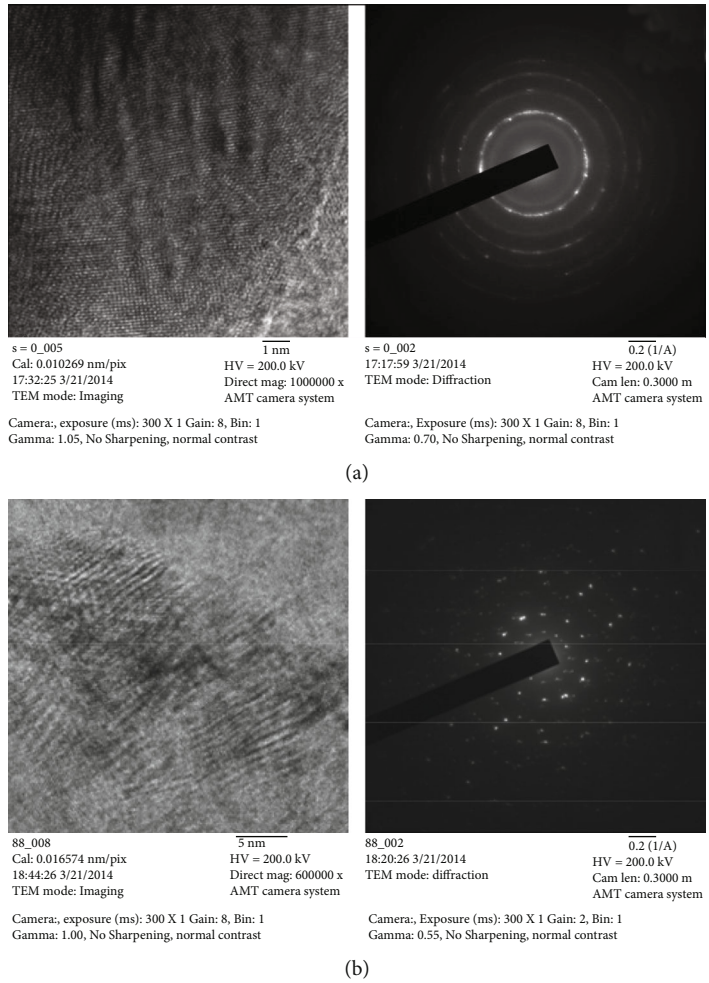

Figure 7: TEM image and TEM diffraction image of as-deposited Fe-Ga alloy films: (a) $R = 0$; (b) $R = 0.07$.

which was unfavorable to increase the magnetostrictive coefficient [26].

Under the experimental conditions in this paper, the gallium content in $Fe_{100-x}Ga_x$ films varies from 14.52 to 16.75, and the sputtering temperature is enough low; therefore, no DO_3 phase appears.

3.3. Domain Structure and Microstructures of Fe-Ga Films. Figure 4 shows that the domain structure was network form, and the domain width of $Fe_{100-x}Ga_x$ films was varied. The magnetic properties of $Fe_{100-x}Ga_x$ films are usually tested by the domain microstructure, and the domain width is an important variable of the domain microstructure.

In Figure 4, the black and white regions are caused by the attractive and repulsive forces between the sample and the magnetic probe. A network form with different resolution and contrast of domain microstructure can be observed.

Additionally, it can be found that the domain width decreases with the decrease of gallium content. The major influence factor is compositions of $Fe_{100-x}Ga_x$ films. The different of compositions leads to different lattice constants of $Fe_{100-x}Ga_x$ films and then the different lattice constant causes

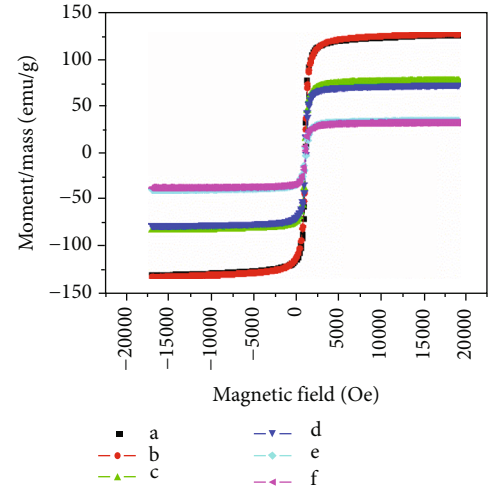

Figure 8: In-plane magnetization vs. magnetic field of $Fe_{100-x}Ga_x$ films with different iron contents.

of different domain widths and different magnetic domain microstructures, thus affecting the magnetostriction properties of $Fe_{100-x}Ga_x$ films.

Table 2: Magnetic results of as-deposited $Fe_{100-x}Ga_x$ films.

Specimen no.	a	b	c	d	e	f
Coercivity (Hci), Oe	45.112	51.864	53.684	55.116	54.977	53.831
Magnetization (Ms), emu/g	127.47	129.13	79.740	74.914	36.613	34.696

It is also found that the magnetic domains become more and more irregular with the decrease of gallium content, which indicates that the magnetic domains of the films are not uniform.

The signal detected by the instrument is the magnitude of the magnetic gradient component in the vertical direction of the membrane surface. When the cantilever oscillates near the surface with its resonance frequency, the resonance frequency of the cantilever will change with the force gradient of the surface in the range of 1 ~ 50 Hz. The instrument used in the experiment detects the change of resonance frequency by means of phase measurement and obtains the distribution of surface force gradient.

As shown in Figure 4, the range of the pin-point phase angle values is shown on the right side of the figure and the corresponding contrast between light and dark in the image. Since MFM can only detect the magnetic gradient component in the vertical direction, the following definitions are made for the different contrasts in the magnetic image: the brighter regions represent the same direction of magnetic moment and the same direction of needle magnetization, which is the positive direction. The darker regions represent the negative direction of the magnetic moment, which is opposite to that of the tip.

Since the magnetic moment has a certain intensity and direction, the contrast of the magnetic force image is related not only to the magnetization but also to the direction of the magnetic moment. In conclusion, the larger the range of phase angle, the larger the detectable magnetic gradient range, the higher the sensitivity of the tip.

Figure 5 shows height difference of the film surface. The height difference increases with increasing iron content in $Fe_{100-x}Ga_x$ films.

Figure 6 shows the variation of height difference with the ratio of the pure iron slice areas to alloy target areas. It can be observed that the surface height difference of the $Fe_{100-x}Ga_x$ films decreases with increasing the value R.

The microstructure TEM images and diffraction image of $Fe_{100-x}Ga_x$ films are shown in Figure 7. There are some strip patterns in the films. Diffraction rings corresponding to polycrystalline appear, so the microstructure of film is crystal structure. However, diffraction rings of specimen no. (f) which iron content is high are not continuous and present a series of rings of dots.

The different diffraction patterns of sample A and sample F are caused by the different compositions in the films. Sample A was sputtered by using an $Fe_{84}Ga_{16}$ target. The film is composed of polycrystalline Fe-Ga alloy grains and a small amount of amorphous Fe-Ga alloy particles. There is no extinction phenomenon during diffraction.

On the contrary, the sample F sputtered films from $Fe_{84}Ga_{16}$ targets covered with Fe slices. The sputtering products have both $Fe_{84}Ga_{16}$ grains and pure iron grains. Due to the lower substrate temperature, the faster sputtering deposition rate, the slower diffusion of iron; not all iron dissolved into Fe-Ga alloy; the films are mainly composed of Fe-Ga alloy grains and a small amount of Fe grains.

Although Fe-Ga alloy grains and pure iron grains are both BCC (A_2), the lattice constants are different, and the diffraction ring is discontinuous because of the structure extinction.

3.4. Magnetization and Coercivity. Magnetization and coercivity results of $Fe_{100-x}Ga_x$ films are shown in Figure 8 and Table 2. The $Fe_{100-x}Ga_x$ films are ferromagnetic. The films with high iron content display large coercivity. The coercivity for the film of specimen no. (a) is 45.112 Oe; it is the minimum value.

It can be explain as follows: there are two factors influence on the coercivity results of $Fe_{100-x}Ga_x$ films, grain size, and film roughness, respectively [5]. Grain sizes are fine in the lower iron content films. The large interface regions can act as pinning centers for domain wall movement. On the other hand, as shown in Figure 5, the film roughness increases with decreasing of iron content. Finally, the coercivity decreases with decreasing iron content.

The larger the coercive force and saturation magnetization, the larger the magnetic loss. According to this principle, if we want to develop magnetostrictive microdevices, we need to prepare thin films with small coercivity.

4. Conclusions

We can conclude that compositions are the key factor that affects alloy phases, grain sizes, film surface roughness, and magnetic domains of the magnetron sputtered $Fe_{100-x}Ga_x$ films. Changing the ratio of the pure iron slice areas to alloy target areas, the desired film composition can be achieved by the improved Mosaic method. The desired film composition was achieved by changing the ratio of the pure iron slice areas to alloy target areas (i.e., the area ratio, R). EDS results of iron content in films are 83.25, 83.61, 84.35, 84.58, 84.95, and 85.58, separately.

The morphologies, magnetic domain structure, microstructure, and compositions of $Fe_{100-x}Ga_x$ films revealed by SEM-EDS, XRD, MFM, VSM, and TEM. The results show that there are <1 1 0> texture in magnetron sputtered $Fe_{100-x}Ga_x$ films. The sharp peak attributed to the A_2 microstructure suggests that the film is crystalline.

The magnetic domain structure of $Fe_{100-x}Ga_x$ films presents a network form, and the domain width decreases with the decrease of gallium content. It is also found that the magnetic domains of the films are not uniform.

The TEM result shows that there are some strip patterns in the films. Diffraction rings corresponding to polycrystalline appear, so the film microstructure is crystal structure. However, diffraction rings of specimen no. (f) which iron content is high are discontinuous because of the structure extinction and present a series of rings of dots.

For a suitable candidate of microdevice applications in MEMS, the optimum composition film should be $Fe_{83.25}Ga_{16.75}$ film.

Data Availability

The data used to support the findings of this study are available from the corresponding author upon request.

Conflicts of Interest

There are no conflicts of interest to disclose for the publication of this paper.

Acknowledgments

This work was supported by the Science Foundation of Education Department of Jiangxi Province of China (No. GJJ201903) and the National Natural Science Foundation of China (No. 51161019).

References

[1] C. Wenzel, B. Adolphi, U. Merkel et al., "Resonant bending sensor based on sputtered Galfenol," *Sensors and Actuators A*, vol. 156, no. 1, pp. 129–133, 2009.

[2] J. W. Yan, J. Pan, and C. S. Zhang, "An overview of magnetostriction Fe-Ga alloy thin films," *Materials Review Supplement*, vol. 1, no. 1, pp. 108–110, 2013.

[3] T. Ueno, E. Summers, M. Wun-Fogle, and T. Higuchi, "Micro-magnetostrictive vibrator using iron-gallium alloy," *Sensor and Actuators A: Physical*, vol. 148, no. 1, pp. 280–284, 2008.

[4] A. Javed, N. A. Morley, and M. R. J. Gibbs, "Structure, magnetic and magnetostrictive properties of as-deposited Fe-Ga thin films," *Journal of Magnetism and Magnetic Materials*, vol. 321, no. 18, pp. 2877–2882, 2009.

[5] H. Basumatary, J. A. Chelvane, D. V. S. Rao, S. V. Kamat, and R. Ranjan, "Influence of substrate temperature on structure, microstructure and magnetic properties of sputtered Fe-Ga thin films," *Journal of Magnetism and Magnetic Materials*, vol. 384, no. 1, pp. 58–63, 2015.

[6] A. Butera, J. Gómez, J. A. Barnard, and J. L. Weston, "Magnetic anisotropy in $Fe_{81}Ga_{19}$/MgO (1 0 0) films sputtered at different powers," *Physica B: Condensed Matter*, vol. 384, no. 1-2, pp. 262–264, 2006.

[7] D. Seguin, M. Sunder, L. Krishna, A. Tatarenko, and P. D. Moran, "Growth and characterization of epitaxial $Fe_{0.8}Ga_{0.2}$/0.69PMN-0.31PT heterostructures," *Journal of Crystal Growth*, vol. 311, no. 12, pp. 3235–3238, 2009.

[8] T. L. Wang, S. S. Feng, and Y. P. Li, "Microstructure and magnetic properties of Fe-Ga thin films," *Rare Metal Materials and Engineering*, vol. 46, no. 2, pp. 406–410, 2017.

[9] A. Niesen, C. Sterwerf, M. Glas, J. M. Schmalhorst, and G. Reiss, "Structural and magnetic properties of sputter-deposited Mn-Fe-Ga thin films," *IEEE Transactions on Magnetics*, vol. 52, no. 7, pp. 1–4, 2016.

[10] J. W. Yan and J. C. Zhou, "Elemental diffusion in Ni-Cr thin films fabricated by double-targets magnetron sputtering," *International Journal of Modern Physics: B*, vol. 21, no. 12, pp. 1981–1996, 2007.

[11] J. W. Yan and J. C. Zhou, "Optimising of strain sensitivity and electric characteristics of Ni-Cr thin film fabricated by magnetron sputtering," *Journal of Material Science & Technology*, vol. 23, no. 2, pp. 195–202, 2007.

[12] D. A. Golosov, S. N. Melnikov, and A. P. Dostanko, "Calculation of the elemental composition of thin films deposited by magnetron sputtering of mosaic targets," *Surface Engineering and Applied Electrochemistry*, vol. 48, no. 1, pp. 52–59, 2012.

[13] J. Yan, R. Zhao, Y. Cha, and Q. Li, "Investigation on microstructures and phases of Fe-Ga alloy films deposited by magnetron sputtering," *International Journal of Nano and Biomaterials*, vol. 9, no. 1/2, p. 95, 2020.

[14] A. Javed, T. Szumiata, N. A. Morley, and M. R. J. Gibbs, "An investigation of the effect of structural order on magnetostriction and magnetic behavior of Fe-Ga alloy thin films," *Acta Materialia*, vol. 58, no. 11, pp. 4003–4011, 2010.

[15] H. LIU, H.-o. WANG, M.-x. CAO et al., "Magnetostriction and microstructure of melt-spun $Fe_{77}Ga_{23}$ ribbons prepared with different wheel velocities," *Transactions on Nonferrous Metal Society of China*, vol. 25, no. 1, pp. 122–128, 2015.

[16] F. Yang, W. D. Fei, and J. Q. Jiang, "Applications of X-ray diffraction technique in the residual stress measurement of films," *Journal of Functional Materials*, vol. 43, no. 11, pp. 1749–1752, 2007.

[17] J.-C. Shih, T.-S. Chin, Z.-G. Sun, H.-W. Zhang, and B.-G. Shen, "Domain structure of TbFe magnetostrictive films by MFM," *IEEE Transactions on Magnetics*, vol. 37, no. 4, pp. 2681–2683, 2001.

[18] H. Z. Song, Y. X. Li, J. T. Zeng, G. R. Li, and Q. R. Yin, "Observation of magnetic domain structure in Terfenol-D by scanning electron acoustic microscopy," *Journal of Magnetism and Magnetic Materials*, vol. 320, no. 6, pp. 978–982, 2008.

[19] Z. G. Sun, H. Kuramochi, M. Mizuguchi, F. Takano, Y. Semba, and H. Akinaga, "Magnetic properties and domain structures of FeSiB thin films prepared by RF- sputtering method," *Journal of Magnetism and Magnetic Materials*, vol. 272-276, pp. 1160-1161, 2004.

[20] Z. Tang, G. Zhao, and T. Ouyang, "Two-phase deep learning model for short-term wind direction forecasting," *Renewable Energy*, vol. 173, no. 72, pp. 1005–1016, 2021.

[21] X. Xu, C. Zhang, H. A. Derazkola, M. Demiral, A. M. Zain, and A. Khan, "UFSW tool pin profile effects on properties of aluminium-steel joint," *Vacuum*, vol. 192, p. 110460, 2021.

[22] X. L. Xu, C. W. Zhang, and H. A. Derazkola, "Dispersion of waves characteristics of laminated composite nanoplate," *Steel and Composite Structures*, vol. 40, no. 3, pp. 355–367, 2021.

[23] J. W. Yan, Y. P. Cha, and Q. P. LI, "The composition analysis and prediction of Fe-Ga alloy films deposited by magnetron sputtering," in *3rd International Conference on Applied*

Mechanics and Mechanical Automation, Phuket, Thailand, 2017.

[24] A. Javed, N. A. Morley, T. Szumiata, and M. R. J. Gibbs, "A comparative study of the microstructural and magnetic properties of textured thin polycrystalline Fe100−xGax (10≤x≤35) films," *Applied Surface Science*, vol. 257, no. 14, pp. 5977–5983, 2011.

[25] R. Q. Wu, "Origin of large magnetostriction in FeGa alloys," *Journal of Applied Physics*, vol. 91, no. 10, pp. 7358–7363, 2002.

[26] A. E. Clark, K. B. Hathaway, M. Wun-Fogle et al., "Extraordinary magnetoelasticity and lattice softening in bcc Fe-Ga alloys," *Journal of Applied Physics*, vol. 93, no. 10, pp. 8621–8623, 2003.